Design of Pauci-Adaptive, Spirally Tiled Mirrors for Large Size Optical Vortex Generation

Gaëtan Fauvel, Philippe Balcou

Design of pauci-adaptive, spirally tiled mirrors for large size optical vortex generation

Gaëtan Fauvel and Philippe Balcou

***Abstract*—We propose the optical design of an adaptive and flexible 4-quadrant, or N-facet, spirally tiled mirror setup, to generate an optical vortex on large diameter laser systems. From a far-field analysis, we derive the optimal angular parameters that generate the highest contents of the targeted Laguerre-Gaussian mode. The modal purities thus obtained are close to those obtained with standard segmented spiral phase plates or mirrors. The intensity behavior in the focal Rayleigh zone is regular, and the effect of a small laser astigmatism, known to break the circularity of the ring intensity profile at focus, can be corrected. This pauci-adaptive faceted mirror setup appears well suited for use on ultra-high intensity or high energy laser systems.**

***Index Terms*—Orbital Angular Momentum, vortex beams, adaptive mirrors, tiled mirrors, high-energy laser beams.**

I. Introduction

LASER beams carrying Optical Angular Momentum (OAM) open fascinating perspectives to trigger and study new phenomena in high field laser-plasma interactions, such as giant magnetic field generation [1], high-order harmonic vortex beam generation [2], orbital control of filamentation [3], direct laser acceleration of electron in the strongly relativistic regime [4], or excitation of complex plasma waves in hot dense plasmas [5]. High intensity and high energy laser/plasma interactions are therefore bound to require means to easily and reliably generate high energy laser beams carrying Orbital Angular Momentum (OAM), and even to be able to control specifically the amount of OAM, as some applications might require a mixture of topological charges in the beam.

Several methods to create OAM beams, such as liquid crystal spatial phase modulators or Gaussian beam mixing at focus, are unfortunately not applicable to intense lasers, as such devices exhibit poor laser damage thresholds. Most prominent is therefore the use of spiral phase plates (SPP) [6], [7]. Ultra-high intensity (few femtosecond, J to kJ class) and high energy (nanosecond, kJ to MJ class) lasers display however specific issues. In the case of high intensity Chirped Pulse Amplification (CPA) lasers, the SPP has to be positioned after the compressor gratings to prevent any damage risk on the latter; therefore the pulse is recompressed, in which case it is advisable not to go through any glass plate, at least for multi-100-TW systems. Longman *et al.* and Bae *et al.* have proposed elegant ways to create a phase spiral on a bending mirror [8], [9]. In the case of high energy lasers, the size of the optics is the obvious issue, as these beams have a width typically in-between 30 cm and 1 m. Although it is possible to ion-etch phase plates of arbitrary size, it would be highly desirable to dispose of an easy and flexible way to create high quality OAM beams of large sizes, for which commercial or technical availability would not be an issue.

In the present article, we propose to use a small number N of conventional mirrors to generate an arbitrary Optical Angular Momentum beam, in a general setup similar to an adaptive mirror, but with a reduced number of degrees of freedom (pauci-adaptive mirrors). From standard propagation equations, we show that the OAM content of the resulting beam can be surprisingly high, even for a small number of mirrors. We also supply an example in which the adaptive nature of the setup can be used to mitigate the deleterious effect of astigmatism in the incident beam.

Most of the following study is devoted to the basic case of a 4-quadrant mirror, or $N = 4$, mostly due to the ease of implementation and high conversion obtained. However, we will switch back to the generic N case whenever general formula can be found.

II. Description of the proposed optical setup

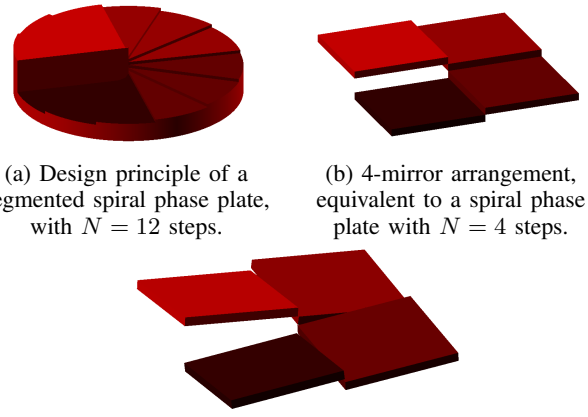

(a) Design principle of a segmented spiral phase plate, with $N = 12$ steps.

(b) 4-mirror arrangement, equivalent to a spiral phase plate with $N = 4$ steps.

(c) 4 tilted mirrors arrangement mimicking a spiral phase plate.

Fig. 1: Transition from a spiral phase plate to an arrangement of four mirrors to induce a quasi-helical wavefront.

Our proposed setup bears features common to adaptive mirrors and to faceted tiled mirrors, as can be found in astronomy. Few proposals have already been brought forward to create OAM beams with adaptive mirrors : Ghai presented

G. Fauvel is with ELI Beamlines Center, Institute of physics of the Czech Academy of Sciences, 25241 Dolni Brezany, Czech Republic. G. Fauvel and Ph. Balcou are with the Université de Bordeaux, CNRS, CEA; Centre Lasers Intenses et Applications, UMR 5107, Talence, France. E-mail: philippe.balcou@u-bordeaux.fr .

a scheme with a piezo device inducing a stress able to bend a circular mirror with a cut into an helix shape [10]; Tyson reported a faceted adaptive mirror with 37 honeycomb-shaped segments, and exhibiting an open aperture of 3.5 mm [11], too small to be of interest for high intensity or high energy lasers.

Figure 1a recalls the typical shape of a spiral phase plate, with N successive steps characterized by an angular span $\theta = 2\pi/N$, and a constant phase value for each step; the step frontiers are straight lines starting from the plate center, in the radial direction.

For $N = 4$, a reflective spiral phase device is strictly equivalent to a set of 4 mirrors, shown in Fig. 1b, with parallel surfaces located at 0, $\lambda/8$, $\lambda/4$, and $3\lambda/8$; these values assume normal incidence, where λ is the central wavelength of the incident laser. Tilting each of the four mirrors with respect to its diagonal axis in the radial direction, as shown in Fig. 1c, results in a setup with an overall close analogy to the SPP ; whether such a setup allows us to create effectively an OAM beam is investigated in the following.

Tiling four square mirrors, or N triangular-shaped mirrors, in a spiral configuration is technically similar to the known and fully mastered method of tiling of grating arrays [12], extensively used for high energy chirped-pulse amplification lasers. Such opto-mechanical devices require a number of high-precision (nanometric) degrees of freedom, whenever separate sub-pupils are to interfere constructively; and also low-precision degrees of freedom, for general positioning and orientation purposes.

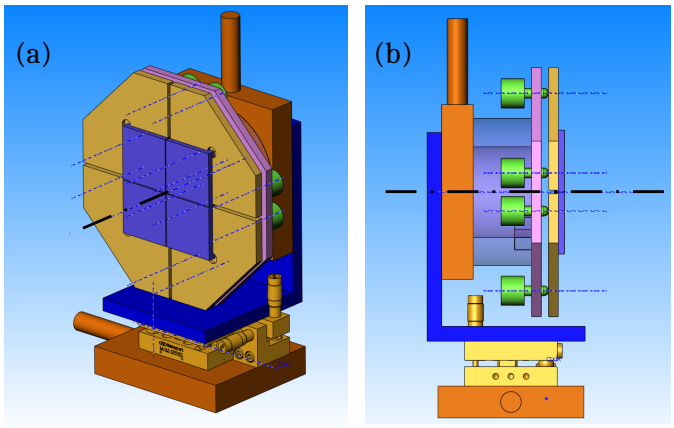

Fig. 2: Prospective front (a) and side (b) views of a 4-quadrant spirally tiled mirror setup.

Figure 2 displays views of a possible implementation of an opto-mechanical 4-quadrant mirror device, featuring low-precision stages and high-precision positioners, eg piezo-electric transducers represented in green, to orient each of the mirrors. Three points are required to pinpoint with nanometric resolution each of the facet planes; this results in a total of 12 high-precision degrees of freedom. From section IV, a global, low-precision rotation around the central axis may also be useful. From standard dimensions of piezo transducers and translation stages, a realistic footprint is around 20 cm squared, making it preferentially usable on large laser beams. Small mirrors can however be located at the center of the optical plane shown in blue, without loss of resolution; conversely much larger mirrors should be implemented without problem.

III. Modeling of Vortex Generation by a Faceted Mirror

Fig. 3 presents the numerical process, whose successive steps follow the path of a modeled laser, from initial laser profile, in intensity and phase, up to the analysis of the output beam vortex content.

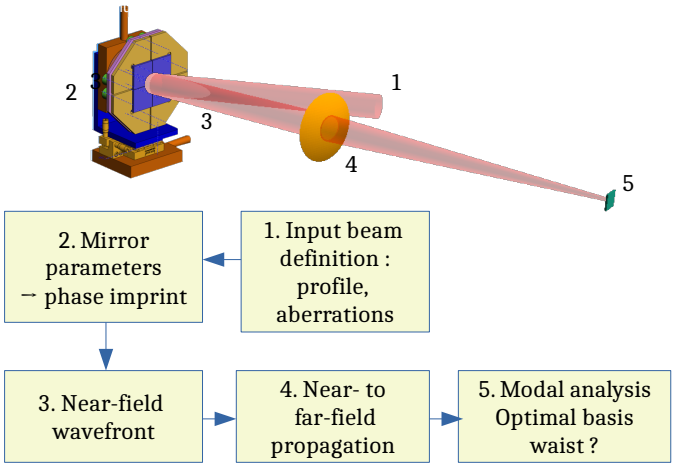

Fig. 3: Sketch of a four-quadrant mirror phase imprint, with the corresponding successive steps of the numerical scheme.

As an input, we consider a laser beam, which we assume to have either perfectly Gaussian TEM_{00} mode, or a super-Gaussian profile. Beam aberrations can be taken into account as a phase function. Experimentally determined beam amplitudes could also be taken as inputs.

In this optical design study, the effect of the four-quadrant mirror is considered as a spatial imprint of a four-quadrant piece-wise bi-linear phase function, derived from orientational parameters presented below. A parabolic phase function models a focusing optical element; the resulting beam is propagated up to the focal plane by a standard Huygens-Fresnel diffraction integral [13]. We then perform the analysis of the modal content of the generated beam in the focal plane. The diffraction integral between the source and focal plane being a linear transform, this modal analysis is possible already in the source plane; however, being able to combine the modal analysis and the examination of the physical distribution of the generated beam in or around the focal plane, where the physical processes of laser/plasma interactions are bound to take place, brings essential physical insights, concerning eg the behaviour in the intermediate field.

A. Definition of quadrant parameters

Figure 4 helps the understanding of the high-precision degrees of freedom required for each mirror quadrant. First we label the quadrant as shown, in the clockwise direction, assuming the observer is facing the faceted mirror.

For each quadrant mirror, the first degree of freedom is the average absolute height of the mirror along the setup normal axis, known as piston, as for standard push adaptive mirrors. A positive piston is taken as corresponding to a shortening of the optical path. A reference position is required to define unambiguously the piston value; we choose as the reference the corner of the mirror, next to the central axis.

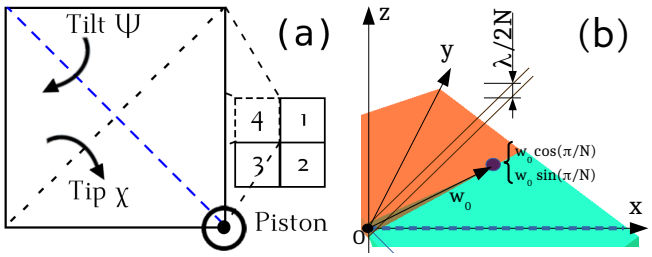

Fig. 4: (a) Definition of a quadrant geometric parameters : diagonal tilt and tip angles, and piston. (b) 3D view of quadrants 4 (brown) and 1 (cyan) in a frame with the x axis along the quadrant 1 diagonal issued from the origin. The z axis is taken along the reflected ray. The central dot shows the position where the heights of both mirrors are equal, for a piston difference of $\lambda/2N$ and a tilt of $-\Psi_0^{(N)}$.

Two orientational angles are also required; we need a definition that follows the four-fold symmetry of the setup. We therefore take as a reference the first diagonal of each quadrant, namely, the diagonal starting from the setup center taken as the origin. For the sake of graphical clarity, we will represent in Fig. 4 the first diagonal of the considered facet as a dashed blue line. This allows us to define tip and tilt angles, which we will call diagonal tip (χ_i) and diagonal tilt (Ψ_i), for mirror i, as shown in Fig. 4a. By convention, we take the diagonal tip to be positive if a normal incident ray on the quadrant is bent towards the central axis; we take the diagonal tilt to be positive if it confers a positive helicity to the reflected ray.

To help writing down the basic geometric calculations, figure 4b displays a 3D representation of facet 1 and of its interface to facet 4, with the origin at the setup center, the (x) axis corresponding to the first diagonal of facet 1, the (y) axis orthogonal to x in the mirror plane, and the overall axis (z) oriented along the reflected ray, (x, y, z) being a direct axis system. Let us now induce a tilt on the quadrant by an angle Ψ, and a tip by an angle χ, both assumed supposed to be very small compared to 1.

To first order, the steering vector of the plane is :

$$\boldsymbol{e} = (-\chi, \Psi, 1) \tag{1}$$

Reminding that we take the central mirror point, or lower left corner here, as the origin O, the plane of each quadrant j follows the equation :

$$-\chi_j x + \Psi_j y + z = h_j. \tag{2}$$

A N-faceted spirally tiled mirror in normal incidence will exhibit a specific rotational symmetry of order N, meaning that a rotation of $2\pi/N$ with respect to the central z-axis should lead to an overall $2l\pi/N$ phase increase upon reflection, modulo 2π. This implies first that all tip and tilt angles, as defined in their own reference frame similar to figure 4, should be identical; and secondly for a given topological value l, that each facet must exhibit a piston of :

$$h_j = \frac{j\ l\ \lambda}{2N}. \tag{3}$$

Non-zero identical values of χ_j will induce a pyramidal phase function, tending to a cone in the limit of high N, similar to an axicon ; this may induce displacements of focal positions, Bessel beam-like behaviours, but is not expected to have any effect on the orbital angular momentum – while possibly opening a way to simple Bessel-like vortex beams. From here on, the tip angles χ_j are therefore set to 0. The pistons being defined by Eq. 3, this leaves the tilt ψ as the essential variable to optimize. A geometric discussion can help figuring out a relevant characteristic tilt value, from which optimisation can start.

Let us consider indeed the frontier between facets 4 and 1 represented in figure 4b, in the reference system already used in which the local x-axis is along the first diagonal of facet 1, ie, the diagonal starting from the origin and represented as a dashed blue line. At the origin, this frontier presents a step $h_4 - h_1$; for ease of the graphical representation, let us assume $l = -1$, and $h_4 = h_1 + \lambda/4N$. At their frontier, a common negative tilt Ψ will decrease the height of facet 4, and increase it for facet 1 as the distance r from the origin increases; the step between the facets will therefore decrease linearly. At some point, the step must come to zero, and becomes negative. w_0^{nf} being the incident beam waist (we note near-field quantities with an ^{nf} superscript), let us define $\Psi_0^{(N)}$ as the tilt for which, at a distance of w_0^{nf} from the origin, the edges of two neighbouring facets have the same height $\lambda/4N$. In Fig. 4b the coordinates of the contact point are $[w_0^{nf}\cos(\pi/N), w_0^{nf}\sin(\pi/N)]$, resulting in :

$$-\psi_0^{(N)} w_0^{nf} \sin(\pi/N) + \lambda/4N = 0. \tag{4}$$

and finally :

$$\psi_0^{(N)} = \frac{\lambda}{4N \sin(\pi/N) w_0^{nf}}. \tag{5}$$

In the cases of $N = 2$ and 4, the angles $\psi_0^{(2)}$ and $\psi_0^{(4)}$ will be used in the following as reference values for the optimal tilts.

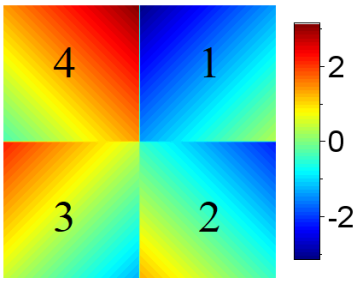

Fig. 5: Example of $l = -1$ phase mask resulting from pistons and diagonal tilts of a 4-quadrant spirally tiled mirror.

As a conclusion to these geometrical considerations, Fig. 5 displays a typical phase mask delivered by a four-quadrant mirror in the following calculations ($l = -1$), as seen again when facing the mirror.

B. Modal analysis of the vortex content

Following the Huygens-Fresnel propagation, the amplitude $\underline{A}_0(r,\theta)$ obtained in the focal plane is analysed on an optimal choice of a Laguerre-Gauss mode basis. Our numerical procedure follows the methods proposed by D'Errico [14], Sanson [2], and Longman [15].

We first recall that a Laguerre-Gaussian $\mathcal{LG}_{p,l}$ mode of amplitude $\underline{u}_{p,l}^{\mathcal{LG}}(r,\theta)$, characterized by two integer numbers p and l under the paraxial, monochromatic, constant linear polarization approximations, reads as :

$$\begin{gathered}\underline{u}_{p,l}^{\mathcal{LG}}(r,\theta) = L_p^{|l|}(\tfrac{2r^2}{w(z)^2}) C_{p,l}^{\mathcal{LG}} \tfrac{(\sqrt{2}r)^{|l|}}{w(z)^{|l|+1}} \times \\ \exp\left[\tfrac{-ikr^2}{2R(z)} - \tfrac{r^2}{w(z)^2} + i(2p+|l|+1)\phi(z) - il\theta\right]\end{gathered} \tag{6}$$

where k is the laser wavevector, $w(z)$ the beam waist size with a minimum waist w_D, $R(z)$ the wavefront curvature, z the distance of propagation with respect to a local focus position z_D, z_R is the Rayleigh length related to w_D, $\phi(z)$ is the Gouy phase, and $L_p^{|l|}$ is a generalized Laguerre polynomial, the expressions for which can be found in textbooks. Here $p+1$ corresponds to the number of rings in the intensity profile, and l is the topological charge, representing the number of periods in the azimuthal phase. These Laguerre-Gaussian modes form a basis with the ortho-normalization formula :

$$\int_0^{+\infty}\int_0^{2\pi} \underline{u}_{p,l}^{\mathcal{LG}*}\underline{u}_{p',l'}^{\mathcal{LG}'} r dr d\theta = \delta_{ll'}\delta_{pp'} \tag{7}$$

One should note that this orthonormalized basis depends on 2 free parameters, w_D and z_D.

From our far-field amplitude $\underline{A}_0(r,\theta)$, we define a α_l^p coefficient as the projection onto the Laguerre-Gauss mode of indices (p,l) :

$$\alpha_l^p = \int_0^{+\infty}\int_0^{2\pi} \underline{A}_0(r,\theta)\underline{u}_{p,l}^{\mathcal{LG}*}(r,\theta) r dr d\theta \tag{8}$$

There is only one term that depends on θ in $\underline{u}_{p,l}^{\mathcal{LG}}$; therefore we can first integrate on θ and then on r :

$$\alpha_l^p = \int_0^{+\infty}\Big(\frac{1}{2\pi}\int_0^{2\pi} \underline{A}_0(r,\theta)e^{il\theta}d\theta\Big) f_{p,l}^*(r) r dr, \tag{9}$$

with

$$\begin{gathered}f_{p,l}^*(r) = 2\pi L_p^{|l|}(\tfrac{2r^2}{w(z)^2}) C_{p,l}^{\mathcal{LG}} \tfrac{(\sqrt{2}r)^{|l|}}{w(z)^{|l|+1}} \times \\ \exp\left[\tfrac{-ikr^2}{2R(z)} - \tfrac{r^2}{w(z)^2} + i(2p+|l|+1)\phi(z)\right]\end{gathered} \tag{10}$$

In the central brackets of equation 9, we recognize a Fourier series expansion :

$$C_l(r) = \frac{1}{2\pi}\int_0^{2\pi} \underline{A}_0(r,\theta)e^{il\theta}d\theta, \tag{11}$$

so that :

$$\alpha_l^p = \int_0^{+\infty} C_l(r) f_{p,l}^*(r) r dr \tag{12}$$

From here it is convenient to define the (p,l) mode purity percentage as the squared modulus of previous equation :

$$P_l^p = |\alpha_l^p|^2 \times 100 \tag{13}$$

Note that the decomposition in l given by (11) is unique [14], as it stems from an azimuthal Fourier series transform; in contrast, the radial decomposition (12) actually depends on the waist size chosen. The obvious idea has long been to use as waist of the $\mathcal{LG}$ basis modes the waist (near-field) w_0^{nf} of the TEM_{00} incident beam. A perfect SPP leads to a conversion efficiency of 78% under this assumption [6] . However Longman and Fedosejevs have pointed out that this default waist value is actually not the most adequate [15]; from analytical calculations, they proposed to use instead w_D^{nf}, given by $w_D^{nf} = w_0^{nf}/\sqrt{|l|+1}$, resulting in a value of 93% for the $\mathcal{LG}_{0\,1}$ purity. The focal plane position does not change.

We choose a global similar approach, with numerical calculations in the far field. The numerical procedure follows all the steps indicated above, with few additional points required to describe the computation flow. The input beam is specified on a cartesian grid, on which all the various phase imprints (aberrations, spiral tiled mirror, focusing) are defined. However, the azimuthal Fourier transform (11) requires the propagated field to be given in polar coordinates; this requires to translate from cartesian to polar, which we do by a standard first order bilinear interpolation on a structured grid.

Once the radial functions (11) are computed by a Fourier integral over θ for each r, we start investigating the optimal new waist that eventually results in the highest component of the target $\mathcal{LG}$ mode, for instance $\mathcal{LG}_{0\,1}$. This is achieved by scanning a range of basis-defining waist values w_D in an interval encompassing the far field TEM_{00} waist w_0, compute the modal content, and choose the w_D value yielding the highest $\mathcal{LG}_{0\,1}$ component. We checked that the second free parameter of the basis of functions, the best focus position along z, remains constant. This can be done at the Huygens-Fresnel stage, by investigating the intensity variations in (x,z) plane in the focal region, and checking that the position along z yielding maximal intensities remains unchanged.

C. OAM laser beam generation optimisation

The whole numerical procedure can now be used to investigate the capability of a 4-quadrant, or N-facet, spirally tiled mirror to generate an OAM beam bearing a target topological charge l. Most of the attention is given to the basic case of $l = 1$ and $N = 4$; however higher angular momenta and other facet numbers will be discussed in a second step.

We made the choice of one specific set of parameters for this series of simulations, to grasp directly the obtained physical values. We therefore use specifications inspired by L4n [16], a frontier high repetition rate nanosecond kiloJoule class laser in Prague. We choose an operating wavelength of λ = 527 nm, with a near-field beam waist size of w_0^{nf} = 247 mm, corresponding for instance to the location of the 4-quadrant mirror in Fig.3, and a focal length f = 2.6 m corresponding to a far-field beam waist at focus of $w_0 \approx 1.8$ μm.

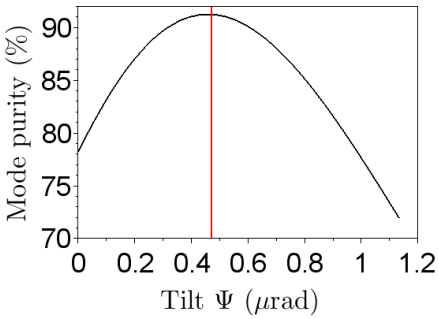

Fig. 6: Optimization of $l = 1$ mode purity with tilt angle Ψ.

Figure 6 shows the modal purity of a $\mathcal{LG}_{0\,1}$ mode as a function of the tilt angle Ψ. Let us remind that $\Psi = 0$ corresponds to a SPP with just four steps, and yields already a purity of 78%; as Ψ is increased, each facet bends towards the inclination of a spiral, increasing the $l = 1$ mode purity. An optimum of 91% is achieved at an angle value Ψ of 4.7×10^{-7} rad, a small but readily achievable value with high precision with piezo-electric positionners and large optics. Decrease in $l = 1$ purity at higher values of Ψ is related to a gradual increase of higher l components. In dimensionless units, we obtain :

$$\Psi_{opt} = 1.25\ \Psi_0^{(4)} \tag{14}$$

Sticking to this Ψ value, we can extract from the calculations the optimal waist w_D that allows the basis $\mathcal{LG}$ family to match as closely as possible the field distribution. Figure 7 shows the modal purity as a function of the tested beam waist w_D. The curve maximum is highlighted by a red line, and is equal to 2.5×10^{-6}m.

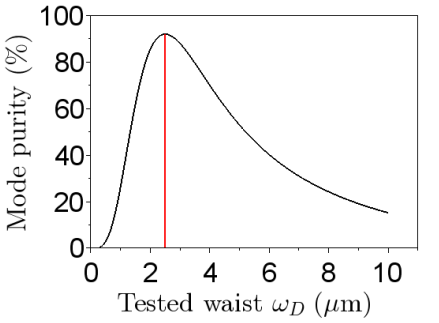

Fig. 7: Optimization of $l = 1$ mode purity at the optimal tilt Ψ as a function of the $\mathcal{LG}$-basis defining beam waist w_D.

To within a small discrepancy, we obtain $w_D = w_0\ \sqrt{|l|+1}$, so that the ratio $\gamma = w_D/w_0$ happens to be numerically the inverse of the Longman result. Indeed, the analysis in [15] is performed in the laser near-field, before any focusing optics; ours is is performed in the laser far-field, at the focus of a lens. The comparison should be hence drawn between the ratio we obtain, and the ratio of near-field divergences, which scale indeed as the inverse of the near-field waists. Our results are therefore consistent with [15], in spite of the specificity of the geometry of spirally tiled mirrors.

Figure 8 displays the intensity and phase distributions obtained in the focal plane, along with color plots of the

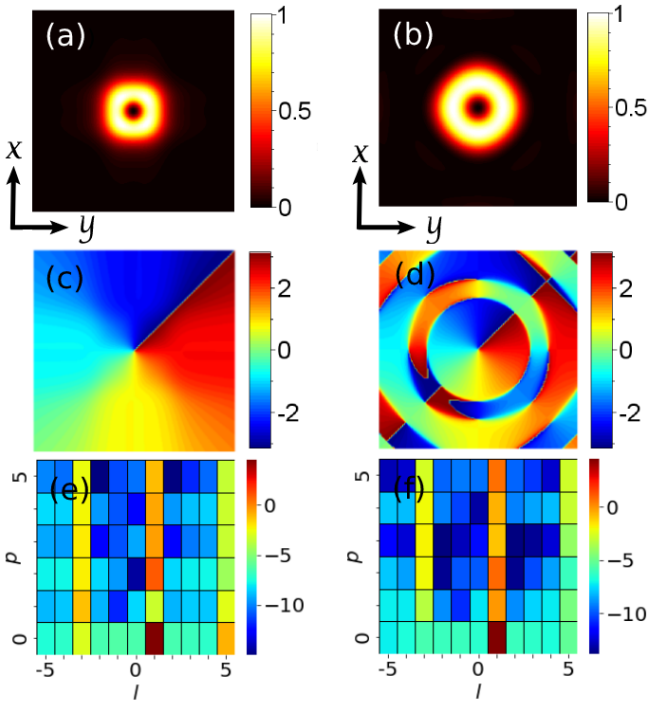

Fig. 8: Normalized intensity profiles at focus (a and b), phase profile at focus (c and d), and modal content matrices of the optical $l = 1$ vortex beam in log color scale (e and f), generated from a perfect Gaussian beam (a,c and e) or from a super-Gaussian beam (b, d and f).

distribution of modes in log scale, with incident Gaussian (a,c,e) or super-Gaussian (b,d,f) beams. Indeed, most high-energy laser facilities use flat-top beams, whose amplitude U_{SG} is commonly described as a super-Gaussian of order 20 :

$$|U_{SG}|^2 = \exp\big(-2(\frac{r^2}{w_0^2})^{20}\big) \tag{15}$$

The Gaussian case leads to a $(0,1)$ purity of 91%; the super-Gaussian to a somehow smaller value of 86%. The number of facets ($N = 4$) is directly visible on the mode decomposition at $l = 1 \pm N$ due to symmetry. However their mode levels are low, with the sum over p of the modes $l = 1 - 4$, or $l = 1 + 4$, both typically at the 1% level, both for the incident Gaussian and super-Gaussian cases. The main secondary mode is consistently the $\mathcal{LG}_{2\,1}$ at 2.5% level. The super-Gaussian leads to stronger components of $l = 1$ and $p >= 3$, typically between 1 and 2%, with a maximum at $p = 5$.

Our approach allows one to explore not only the focal plane but the entire focal region ; figure 9 thus presents the normalized plot intensity distribution in the (x, z) plane. The characteristic intensity hollow on axis appears clearly, with no spurious feature up to 10 Rayleigh lengths, a strong indication that the scheme can be used eg for direct electron acceleration.

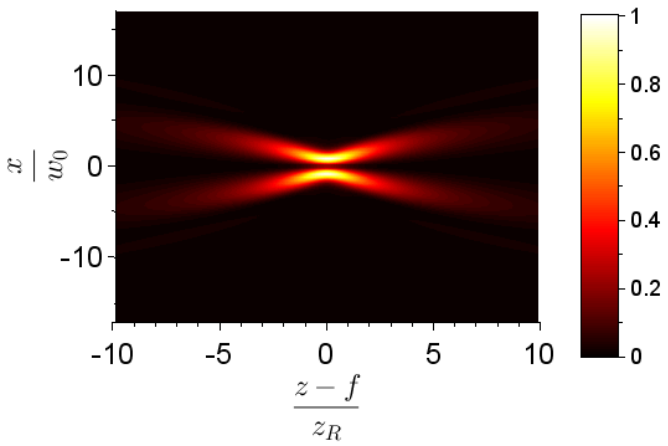

Fig. 9: Normalized intensity distribution in an axial plane (x, z) of the focal region. z axis in units of Rayleigh ranges.

We now explore whether changing the number of facets can be of interest. Let us first consider the specific case of 2 facets; indeed, a $l = 1$ mode purity of 82% can already be obtained with only two mirrors, at a tilt value of 1.10 $\Psi_0^{(2)}$. While clearly lower than the figures presented with $N = 4$, this is already sufficient to be of interest, considering the improved ease of an experimental implementation.

Conversely, high-N values are of interest to reach high l values. Table I shows the evolution of the optimal $\mathcal{LG}_{05}$ mode purity, as a function of N and of the incident beam profile. The purity can be seen to increase steadily, then to saturate to a value close to the perfect SPP one.

Number of facets (N)	5	8	10	12	14	SPP
$\mathcal{LG}_{05}$ purity (incident TEM_{00})	54	63	65	66	67	68
$\mathcal{LG}_{05}$ purity (super-gaussian)	71	78	80	81	82	83

TABLE I: Mode purity as function of the number of facets N for l=5, and comparison with the case of a perfect SPP.

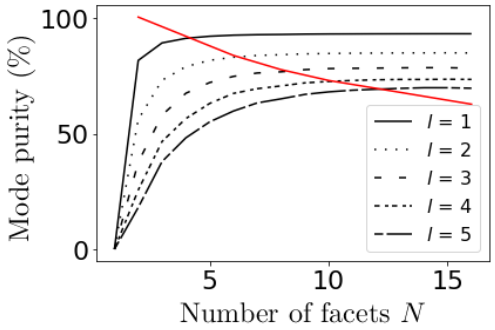

Fig. 10: Evolution of the mode purity for different topological charges as function of the number of facets N. The intersection between the red line and mode purity curves, shows the mode purity reached corresponding to a number of facets $N = 2l+2$.

Let us take as criterium for this saturation to happen at an optimal facet number N_{opt}, the fact that the incremental purity improvement between N_{opt} and $N_{opt}+1$ is 1% or less. Figure 10 shows a series of purity curves as a function of the number N of facets for different values of the target topological charge l; the red thick curve connects the N_{opt} values thus defined. This curve corresponds to an empirical linear law :

$$N_{opt} = 2l + 2. \tag{16}$$

Figure 11 makes use of this empirical law to show the mode purity achieved as a function of the target topological value l (bottom x-axis), the facet number $N(l)$ being given by equation (16) (top x-axis). Table II completes Fig. 11 by displaying the numerical purity values for the most important, five lowest l values. For a supergaussian beam, the optimal target mode purity is seen to remain at high values, above 80% up to l =10; conversely, a gaussian beam starts from the highest possible value of 91% for $l = 1$, and then decreases steadily down to 60% in the same range. This shows that the beam areas far from the optical axis play an important role in the vortex formation by a spirally tiled mirror; for high l values, the scheme is therefore particularly suitable to top-hat laser profiles, typical of high energy lasers.

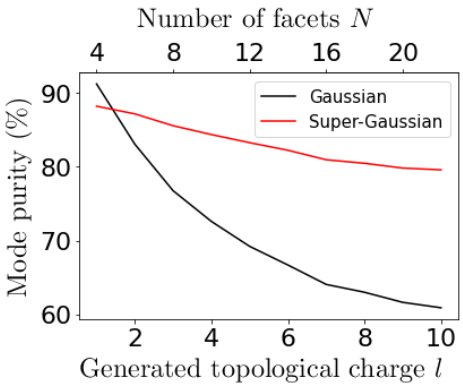

Fig. 11: Evolution of the mode purity as function of the topological charge l using a number of facets $N = 2l + 2$ for a Gaussian beam (black line) and a super-Gaussian (red line).

Topological charge (l)	1	2	3	4	5
Optimal number of facets (N_{opt})	4	6	8	10	12
Mode purity % (incident TEM_{00})	91	82	75	70	66
Mode purity % (superGaussian)	88	87	85	83	81

TABLE II: Mode purity of high-l OAM beams generated thanks to $(2l + 2)$-facet spirally tiled mirrors.

IV. Adaptive Mitigation of the Ring Symmetry Breakdown Due to Astigmatism

In addition to the static phase imprint designed to induce an optical vortex, the four-quadrant mirror can be exploited as an adaptive mirror, although with fewer degrees of freedom than conventional adaptive mirrors – so that it can be qualified of pauci-adaptive mirror. We investigate here how this capability may be of interest to generate regular vortex beams when the incident bears the most common low-order aberration, namely, astigmatism.

Astigmatism is indeed a serious problem to generate vortex beams; it has been known since Bekshaev et al. [17] that

astigmatism in the beam incident on the SPP induces a breakdown of the cylindrical symmetry of the ring-shaped intensity profile at focus, even for small astigmatisms. A typical two-lobe shape can then be observed, oriented at 45° from the axis of astigmatism. This has potentially severe consequences, especially when the physical process taking place at focus has a non linear dependence with intensity [18], [19].

This behavior can be understood by considering the phase function of astigmatism, which, in polar coordinates (r, θ), may be written as :

$$\Phi_a(r,\theta) = \alpha_a \sqrt{6} \cos(2\theta - \beta_a) r^2 / w_0^2 \qquad (17)$$

where α_a is a Zernike polynomial coefficient, and β_a is the orientation of the aberration, usually 0° or 45° in a Zernike development. Due to the $\cos(2\theta)$ term, this phase function mixes the initial laser spatial mode, assumed to have null angular momentum, with angular momentum side-bands of orders ± 2. However, this phase function does not modify the intensity, meaning that the angular momentum side-bands are in phase quadrature with the main $\mathcal{LG}_{0\,0}$ beam component. This phase relationship changes upon transmission or reflection on the spiral phase optics, and subsequent propagation to the focus, as the different l acquire l-dependent phases, bringing the sidebands in phase with the new dominant $\mathcal{LG}_{0\,1}$ component, leading to angularly dependent interferences. Figure 12a illustrates this discussion, by displaying the intensity profile obtained at focus from an initial $\mathcal{LG}_{0\,1}$ beam, on which the astigmatic phase of Eq. 17 is imprinted, with $\alpha_a = 0.1$ and $\beta_a = 0$.

In contrast to conventional adaptive mirrors, featuring a high number of actuators and smooth phase imprint, our proposed pauci-adaptive tiled-mirror setup is not able to remove exactly the phase profile of astigmatism; however, it can induce angular momentum side-bands, that can be chosen to play with, and hopefully mitigate pre-existing interferences between angular momentum modes.

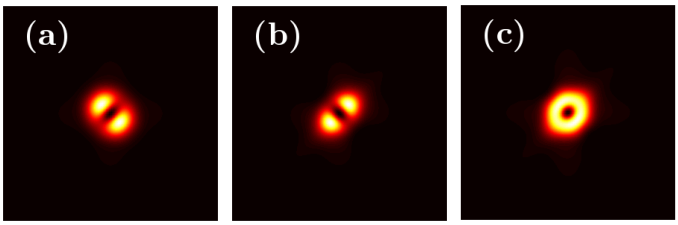

Fig. 12: (a) Two-lobe structure from an incident astigmatic beam (parameters : $\lambda = 0.63$ μm, $z_R = 0.9$ mm; $\alpha_a = 0.1$,$\beta_a = 0$). (b) Two-lobe structure from a π-crown phase imprint $\delta\phi$ ($\delta\phi_c = 0.4$, $\beta_c = 45°$). (c) Corrected vortex beam, when both phase imprints are added.

To illustrate this strategy, we choose the most simple function to impose $l = \pm 2$ sidebands by a four-quadrant mirror, by playing with the piston degrees of freedom h of the quadrants : $h_1 = h_3 = +h_c, h_2 = h_4 = -h_c$, where $h_c = (\lambda/4\pi)\ \delta\phi_c$ and $\delta\phi_c$ is the phase retardance of the first quadrant. The phase imprint has a periodicity of π rad; to help the understanding, we will call this phase function a π-crown phase.

Figure 12b shows the resulting outlook of the intensity profile at focus, with $\delta\phi_c = 0.4$ rad and an orientation $\beta_c = 45°$. A double lobe structure appears indeed, very similar to the one induced by astigmatism, both being essentially the visual result of the existence of the interference with in-phase $l = \pm 2$ sidebands. The crossed axis between the lobes stems from our choice of the orientation angle β_c, and of a positive $\delta\phi_c$ piston phase.

Figure 12c shows the final focus intensity profile, when both the astigmatism saddle-like phase of equation 17, and the π-crown phase corresponding to Fig. 12b are imprinted on the wavefront. The ring outlook appears mostly restored; numerically we noted that this happens when the components of ($p = 1$,$l = -1$) and ($p = 1$,$l = 3$) display balanced values. The ($p = 0$,$l = 1$) mode purity decreases to 86% in this case. This illustrates the obvious drawback of the imprint of such a π-crown phase : high to very-high spatial modes are excited by the additional wavefront discontinuities, so that the mitigation of low-order defects comes at the expense of a loss of energy into high-order defects. However, from an experimentalist point of view, it may be advantageous to lose few percents of energy, but have the flexibility to mitigate the effect of a small astigmatism, and improve the overall circular symmetry of the intensity ring. Indeed, most laser systems benefit from at least one adaptive mirror, so that the final astigmatism in the beam is bound to be small – which is the right condition for this additional correction method to apply efficiently, with limited energy loss to high spatial orders.

The π-crown phase is not the only one that can be implemented on a pauci-adaptive 4-quadrant mirror; basically any interplay with piston, diagonal tips and tilts with a period of π rad will excite $l = \pm 2$ sidebands. N-angular facet mirrors, eg. with N=6, might also be used to mitigate the effects on vortices of higher order aberrations, such as trifoil. Such discussions are beyond the scope of this work.

V. Conclusion

In this optical design study, we have investigated numerically whether a proposed new optical setup, based on N tiled mirrors in a spiral configuration, can generate efficiently optical vortex beams. We have explored in particular the case of 4-quadrant mirrors; the results are very promising, as the phase imprints based on the facet piston and diagonal tilt degrees of freedom allow one to reach modal purities of $\mathcal{LG}_{0\,1}$ up to 91%, starting from a pure TEM_{00} Gaussian beam, and 86% with a super-Gaussian beam. The former value obtained thanks to this simple and flexible device is close to the 93% optimal conversion predicted on a perfect spiral phase plate or mirror.

Other values of target orbital angular momentum and other numbers of facets were also explored : N=2, or higher N values to generate OAM beams of higher topological charges. The main applicability of the proposed setup remains however the case of a 4-quadrant mirror, used to generate charges l of 1 or 2.

From an experimental point of view, the 4-quadrant spirally tiled mirror may offer a host of practical advantages :

1) it can be implemented on the basis of commercial square mirrors of arbitrary size, with any coating, making it ideal for large-size beams, for which provision of a spiral phase plate or mirror may be difficult;
2) the incidence angle can be chosen at will;
3) it is easily tunable and can generate different topological charge values at will, without any setup overhaul. High topogical charges can be obtained on the basis of setups with higher facet numbers;
4) any damaged mirror can be replaced individually;
5) generation of fractional vortex orders, resulting in a controlled mix of Laguerre-Gaussian modes, can be explored;
6) finally, this pauci-adaptive setup can be used as a last-resort adaptive mirror, to provide fine adjustments and corrections of angular momentum side-modes, known to impair the vortex intensity profile at focus.

From this optical study, several pathways exist for a practical implementation, and for the definition of optical alignment procedures. In this respect, our proposed setup should benefit from the experience of previous works on tiling of mirrors in large area telescopes, or tiling of diffraction gratings in CPA lasers. Successful implementations would be highly beneficial to develop a fascinating new field within laser-plasma physics : the coupling of ultra-intense or high-energy optical vortices and magnetic fields in hot plasmas [1], [4], [5].

ACKNOWLEDGMENT

G. Fauvel thanks the Institute of Physics of the Czech Academy of Sciences for funding. The authors also thank the Light S&T Ecole Universitaire de Recherche for financial support, Ms Lise Brigot and Ms Julie Camus for their help, R. Bouillaud, L. Merzeau, G. Corde and R. Ferrère for technical and computational support.

REFERENCES

[1] R. Nuter, P. Korneev, I. Thiele, and V. Tikhonchuk, "A plasma solenoid driven by an Orbital Angular Momentum laser beam," *Physical Review E*, vol. 98, no. 3, p. 033211, Sep. 2018, arXiv: 1804.03574.
[2] F. Sanson, A. K. Pandey, F. Harms, G. Dovillaire, E. Baynard, J. Demailly, O. Guilbaud, B. Lucas, O. Neveu, M. Pittman, D. Ros, M. Richardson, E. Johnson, W. Li, Ph. Balcou, and S. Kazamias, "Hartmann wavefront sensor characterization of a high charge vortex beam in the extreme ultraviolet spectral range," *Opt. Lett.*, vol. 43, no. 12, pp. 2780–2783, Jun 2018.
[3] E. V. Vasilyev, S. A. Shlenov, and V. P. Kandidov, "The multifocus structure of radiation upon femtosecond filamentation of an optical vortex in a medium with an anomalous group velocity dispersion," *Optics and Spectroscopy*, vol. 126, no. 3, pp. 16–24, 2019.
[4] D. R. Blackman, R. Nuter, P. Korneev, and V. T. Tikhonchuk, "Nonlinear Landau damping of plasma waves with orbital angular momentum," *Phys. Rev. E*, vol. 102, p. 033208, 2020.
[5] Y. Shi, D. R. Blackman, D. Stutman, and A. Arefiev, "Generation of ultra-relativistic monoenergetic electron bunches via a synergistic interaction of longitudinal electric and magnetic fields of a twisted laser," *Physical Review Letters*, vol. 126, p. 234801, 2021.
[6] M. W. Beijersbergen, R. P. C. Coerwinkel, and M. Kristensen, "Helical-wavefront laser beams produced with a spiral phase plate," *Optics Communications*, p. 7, 1994.
[7] K. Sueda, G. Miyaji, N. Miyanaga, and M. Nakatsuka, "Laguerre-Gaussian beam generated with a multilevel spiral phase plate for high intensity laser pulses," *Opt. Express*, p. 6, 2004.
[8] A. Longman, C. Salgado, G. Zeraouli, J. I. Apiñaniz, J. Antonio Pérez-Hernández, M. K. Eltahlawy, L. Volpe, and R. Fedosejevs, "Off-axis spiral phase mirrors for generating high-intensity optical vortices," *Optics Letters*, vol. 45, no. 8, p. 2187, Apr. 2020.
[9] J. Y. Bae, C. Jeon, K. H. Pae, C. M. Kim, H. S. Kim, I. Han, W.-J. Yeo, B. Jeong, M. Jeon, D.-H. Lee, D. U. Kim, S. Hyun, H. Hur, K.-S. Lee, G. H. Kim, K. S. Chang, I. W. Choi, C. H. Nam, and I. J. Kim, "Generation of low-order Laguerre-Gaussian beams using hybrid-machined reflective spiral phase plates for intense laser-plasma interactions," *Results in Physics*, vol. 19, p. 103499, Dec. 2020.
[10] D. Pal Ghai, P. Senthilkumaran, and R. S. Sirohi, "Adaptive helical mirror for generation of optical phase singularity," *Applied Optics*, vol. 47, no. 10, p. 1378, Apr. 2008.
[11] R. K. Tyson, M. Scipioni, and J. Viegas, "Generation of an optical vortex with a segmented deformable mirror," *Applied Optics*, vol. 47, no. 33, p. 6300, Nov. 2008.
[12] A. Cotel, M. M. Castaing, P. P. Pichon, and C. Le Blanc, "Phased-array grating compression for high-energy chirped pulse amplification lasers," *Optics Express*, vol. 15, no. 5, 2007.
[13] E. Hecht, *Optics*, 4th ed. Addison Wesley, 2002.
[14] A. D'Errico, R. D'Amelio, B. Piccirillo, F. Cardano, and L. Marrucci, "Measuring the complex orbital angular momentum spectrum and spatial mode decomposition of structured light beams," *Optica*, vol. 4, no. 11, p. 1350, Nov. 2017.
[15] A. Longman and R. Fedosejevs, "Mode conversion efficiency to Laguerre-Gaussian OAM modes using spiral phase optics," *Optics Express*, vol. 25, no. 15, p. 17382, Jul. 2017.
[16] N. Jourdain, U. Chaulagain, M. Havlík, D. Kramer, D. Kumar, I. Majerová, V. T. Tikhonchuk, G. Korn, and S. Weber, "The L4n laser beamline of the P3-installation: Towards high-repetition rate high-energy density physics at ELI-Beamlines," *Matter and Radiation at Extremes*, vol. 6, no. 1, p. 015401, Jan. 2021.
[17] A. Y. Bekshaev, M. S. Soskin, and M. V. Vasnetsov, "Optical vortex symmetry breakdown and decomposition of the orbital angular momentum of light beams," *Journal of the Optical Society of America A*, vol. 20, no. 8, p. 1635, Aug. 2003.
[18] F. Sanson, A. K. Pandey, I. Papagiannouli, F. Harms, G. Dovillaire, E. Baynard, J. Demailly, O. Guilbaud, B. Lucas, O. Neveu, M. Pittman, D. Ros, M. Richardson, E. Johnson, W. Li, Ph. Balcou, and S. Kazamias, "Highly multimodal structure of high topological charge extreme ultraviolet vortex beams," *Optics Letters*, vol. 45, no. 17, p. 4790, Sep. 2020.
[19] J. Courtial, K. Dholakia, L. Allen, and M. J. Padgett, "Second-harmonic generation and the conservation of orbital angular momentum with high-order Laguerre-Gaussian modes," *Phys. Rev. A*, p. 4, 1997.

Dr Philippe Balcou is Directeur de Recherches at CNRS, France. He graduated from Ecole Polytechnique in 1989, received a PhD in optical and quantum physics from Université Pierre et Marie Curie in 1993. He was interim director of Laboratoire d'Optique Appliquée in 2003-2004, director of the Centre Lasers Intenses et Applications from 2007 to 2016. He is currently member of the Scientific Council of CNRS. He received the 2002 Aimé Cotton prize for his contributions to the physics of high harmonic generation and attosecond science.

Fauvel Gaëtan received the Bachelor of Science degree with honours in physics in 2020, the Master of Science degree with high honours in 2022 from the Light S&T graduate program at the University of Bordeaux, France with a focus on the generation of intense laser beam carrying an orbital momentum and X-ray spectroscopy. Currently, he is pursuing a PhD at ELI Beamlines, Czech Republic on gamma generation under the supervision of Dr. Condamine, funded by the first NSF-GACR project.